A novel framework to study the effect of tree architectural traits on stemflow yield and its consequences for soil-water dynamics

Gonzalez-Ollauri, Alejandro; Stokes, Alexia; Mickovski, Slobodan B.

Published in:
Journal of Hydrology

DOI:
10.1016/j.jhydrol.2019.124448

Publication date:
2020

Document Version
Author accepted manuscript

A novel framework to study the effect of tree architectural traits on stemflow yield and its consequences for soil-water dynamics

Alejandro Gonzalez-Ollauri[1,3] Alexia Stokes[2], Slobodan B. Mickovski[1]
[1]The BEAM Research Centre, School of Computing, Engineering and Built Environment, Glasgow Caledonian University, G4 0BA Glasgow, UK
[2] INRA, AMAP, CIRAD, IRD, CRS, University of Montpellier, 34398 Montpellier Cedex 5, France
[3]Corresponding author: alejandro.ollauri@gcu.ac.uk ; gollauri@gmail.com

Abstract

A novel experimental approach and numerical framework are proposed to study the effect of tree architectural traits on stemflow yield and its effects on soil-water dynamics. The framework includes a data mining workflow employing information from two experimental steps: (i) evaluation of the effect of tree aboveground architecture on stemflow yield and (ii) quantification of specific parameters for soil-water dynamics with and without stemflow. We studied double-funnelling (stemflow and root-induced preferential flow) under three sycamore (*Acer pseudoplatanus* L.) trees growing on a slope in Scotland during the summer season and measured architectural traits. Stemflow yield ranged from 1.3 to 3.8 % of the incident rainfall, with funnelling ratios of between 2.2±2.1 and 5.2±3.9. Double-funnelling to a depth of up to 400 mm beneath the soil surface occurred as matrix flow and was significantly and positively correlated with the vertical root distribution. Soil-water dynamics were distinctly different with and without stemflow. Our framework revealed that the number of tree branches, their insertion angle, leaf number, and stem basal diameter influenced stemflow yield within rainfall thresholds of 1.1 and 3.5 mm d^{-1}. The framework also showed that stemflow yield had a negative impact on soil matric suction, while air temperature was the most influential covariate affecting soil-water dynamics, likely due to its strong correlation to evapotranspiration during the summer season. In spite of the study limitations, such as small sample size and differences between individuals, we show that the proposed framework and experimental approach can contribute to our knowledge of how stemflow generated aboveground triggers major responses in soil-water dynamics belowground.

Keywords: temperature, soil moisture, matric suction, preferential flow, sycamore

1. Introduction

Stemflow is a poorly studied hydrological process that occurs mostly in woodland ecosystems (Levia and Germer, 2015). Stemflow comprises the funnelling of incident precipitation around the tree stem, with subsequent flow occurring along roots and into soil pores (i.e. double-funnelling; Johnson and Lehmann, 2006). Stemflow has been overlooked due to its point-source nature and its apparently small contribution to the water cycle (Levia et al., 2011). However, many geoscientists now acknowledge the potential role of stemflow in the regulation of hydrological and biogeochemical cycles in forests and shrublands (Levia and Germer, 2015).

Stemflow generally represents 1 to 20 % of incident precipitation (Levia and Frost, 2003). But, in reality, a substantial volume of water can concentrate around the tree bole in a single precipitation event (e.g. Gonzalez-Ollauri and Mickovski, 2017a). Stemflow is formed in the forest canopy, and recent work has strived to unveil how canopy architecture can regulate the formation of stemflow before being funnelled belowground (e.g. Levia et al., 2010, 2015; Bialkowski and Buttle, 2015; Yuan et al., 2017; del Campo et al., 2018). However, tree architecture is complex (e.g. Barthélémy and Caraglio, 2007; Côté et al. 2011), and varies with tree age (e.g. Meinzer et al., 2011), and across species and biomes (e.g. Wright et al., 2005; Kattge et al., 2011). Outcomes from advanced data mining frameworks (e.g. Torgo, 2011) could have important applications in the elucidation of strategies by practitioners seeking to control relevant phenomena that are regulated through stemflow (e.g. groundwater recharge and nutrient cycling, Levia et al., 2011; del Campo et al., 2014; 2018).

Double-funnelling results into various modes of subsurface flow, e.g.preferential flow, bypass flow and matrix flow (Liang et al., 2011; Spencer and van Meerveld, 2016), or even surface runoff (Herwitz, 1986; Miyata et al., 2009). Tracking double-funnelling is labour-intensive (e.g. Liang et al., 2011; Germer, 2013; Spencer and van Meerveld, 2016), and it is difficult to identify the subsurface flow mode, its potential drivers, and the subsequent effect in the soil. For trees growing on slopes, stemflow is funnelled towards the downslope part of the stem and soil (Liang et al., 2011; Spencer and van Meerveld, 2016), where macropores and gaps between the root and soil channel this subsurface flow (Martinez-Meza and Whitford, 1996; Schwärzel et al., 2012; Spencer and van Meerveld, 2016). There is little convincing information, however, indicating whether the subsurface flow mode associated to double-funnelling is species-specific and season-dependent, or whether it changes with

meteorological conditions, e.g. rainfall intensity or inter-rainfall interval (van Stan et al., 2012; Tanaka et al., 2017). The subsurface flow mode may also depend on soil characteristics, such as moisture content and texture, as well as plant root density. In spite of the advances made over the last decade to generate knowledge on how soil hydrology is impacted by stemflow (for review, see Levia and Germer, 2015), linking double-funnelling and subsequent changes to soil-water dynamics in response to meteorological events has not yet been attempted.

Changes in soil moisture and matric suction related to double-funnelling can help to clarify what level of stemflow yield leads to noticeable hydrological responses in soil. Measuring soil hydrological variables also allows an assessment of whether double-funnelling occurs along the same soil paths repeatedly, and whether it influences mechanical stresses in soil, that could then affect how vegetation protects against rainfall-induced, shallow landslides (Gonzalez-Ollauri and Mickovski, 2017a,b). Changes in soil temperature at zones with signs of double-funnelling may also indicate the arrival of water and nutrients transported from the canopy to soil (e.g. Germer et al., 2012), that in turn alter soil microbial activity (McClain et al., 2003; Kuryakov and Blagodatskaya, 2015; Rosier et al., 2016). However, studying soil-water dynamics influenced by stemflow is experimentally challenging and data are difficult to analyse. Therefore, robust experimental and numerical frameworks should enable us to overcome these problems and so elucidate relationships between stemflow and soil-water dynamics.

The aim of our study is to propose a novel experimental approach and numerical framework to estimate how aboveground tree architecture affects stemflow yield and, subsequently, soil-water dynamics. Our objectives are: (i) evaluation of the effect of aboveground tree architecture on stemflow yield; (ii) identification of soil-root zones subjected to double-funnelling; (iii) quantification of soil moisture, matric suction and soil temperature with and without stemflow and (iv) evaluation of the effect of two external meteorological variables (i.e. rainfall and air temperature) on soil-water dynamics in contrast with stemflow yield. To achieve these objectives, we studied double-funnelling and its effect on soil-water dynamics under sycamore (*Acer pseudoplatanus* L.) trees. Sycamore is a deciduous, broadleaf, fast-growing tree with a broad, domed crown and smooth bark (Pasta et al., 2016). Mature sycamores are very resistant to wind loading, coastal exposure, and pollution, and these features make it a useful species for protecting slopes against landslides, erosion, and rockfall

(Norris et al. 2008). Therefore, sycamore is a potentially useful species in protection forests and on unstable slopes. Understanding how the architectural traits of sycamore affect soil hydrological characteristics will allow a full assessment of the utility of this species for ecological engineers.

2. Materials and Methods

2.1. Tree individuals and study site

The study site was located adjacent to Catterline Bay, Aberdeenshire, UK (WGS84 Long: -2.21 Lat: 56.90; supplementary material Fig. S1a), within the temperate humid climate zone (Cgc: subpolar oceanic climate; Köppen, 1884). The mean annual temperature over the period 2011 – 2018 was 8.9 °C and the mean annual rainfall was 556.8 mm (voor de Poorte, 2018). The precipitation at the site is characterised by frequent, low-intensity rainfall events (Gonzalez-Ollauri and Mickovski, 2016; 2017a) and the prevailing wind is south-westerly. Three adjacent sycamore (*Acer pseudoplatanus* L.) individuals (Syc1, Syc2, and Syc3), that were approximately 40 years old, were chosen for the study (Fig. S1b). The stand was established on a 20.3±11.6° southwest facing slope, oriented 260-280° from due north. Soil is well-drained (saturated hydraulic conductivity: 7.1e-05 m s^{-1}), with a soil organic matter content of 12.4 %. Landslide prone silty sands (sand: 66.8 %; silt: 1.4 %; clay: 0.8 %) overlie conglomerate rock. The topsoil at the site (to a depth of 600 mm beneath the soil surface) had a mean dry bulk density of 1.3 g cm^{-3}, a drained cohesion of 30.5 kPa, a mean angle of internal friction of 19.4°, and a specific gravity of 2.6.

2.2. Aboveground tree architectural traits

The aboveground architecture of the tree individuals was characterised with 13 readily measurable traits reported to influence stemflow yield (Levia et al., 2015; Fig. 1). A surveyors' meter tape was used to measure: (i) the tree's basal area or diameter at breast height (*DBH*; m) and (ii) the projected canopy-crown area (C_A; m^2) according to Spoke's distance method (Blozan, 2008), assuming a circular crown projection on the ground surface. A spherical crown densiometer was used to estimate (iii) the canopy cover fraction (*c*; %; Lemon, 1956). (iv) Tree height (*Ht*; m) was measured from an upslope position with a Leica®

laser meter. (v) The leaf area index (*LAI*) was estimated with the Wolf et al. (1972) direct method. A hand-held inclinometer was used to measure (vi) the stem lean from the vertical (S_L; °), (vii) the maximum branch insertion angle from the horizontal ($_{mx}Br_a$; °), and (viii) the mean branch insertion angle above the horizontal ($_{av}Br_a$; °). (ix) The number of primary (*PBr;* developing directly from the main stem) and (x) secondary branches (*SBr;* borne directly on the primary branches) were counted manually to then calculate the branch count per unit projected area of tree crown (Levia et al., 2015). Finally, (xi) the total number of leaves (nL; m^{-2}), (xii) leaf biomass (L_{BM}; g m^{-2}), and (xiii) branch biomass (Br_{BM}; Kg m^{-2}) per unit projected area of tree crown was estimated through a destructive method that involved cutting a primary and two secondary branches from a fourth, unstudied, sycamore individual. Leaves were counted and, along with woody parts, were oven-dried at 60°C until a constant mass was reached.

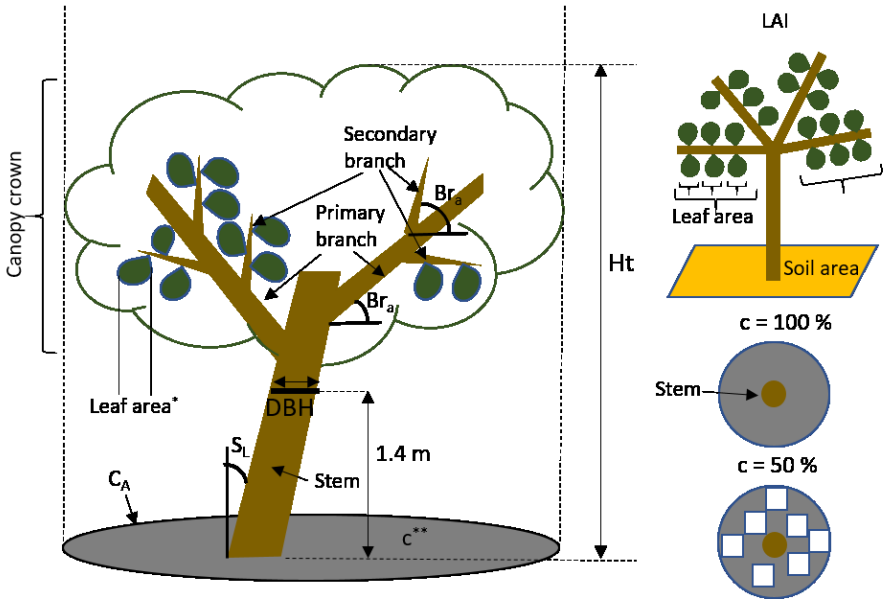

Figure 1. Illustration showing tree architectural traits measured in this study. *DBH*: diameter at breast height; C_A: projected canopy-crown area; c: canopy cover fraction; *Ht*: tree height; *LAI*: leaf area index; S_L: stem lean; Br_a: branch insertion angle. On the right-hand side, the concept of *LAI* and two *c* examples are illustrated, i.e. dense canopy crown with *c*=100 % and sparse canopy crown with *c*=50%, where the white squares portray the penetration of sunlight through the canopy.

2.3. Double-funnelling and subsurface flow

To identify the zones where double-funnelling results in an accumulation of subsurface flow, on 18/06/2018, we sprayed 20 l of a dye solution (i.e. Brilliant Blue FCF; 5 g l^{-1}) between ground level and a height of 1.7 m on the downslope side of the stem (Laing et al., 2011; Nespoulous et al., 2019) on two of the sycamore individuals (Syc1 and Syc2; Fig. 2b). For this, we used a 20 l backpack sprayer for 35 minutes per individual, corresponding to a

precipitation intensity of 45.7 mm h^{-1}. Before we sprayed the dye solution, we used a moisture profile probe (Delta-T®) to measure the mean soil volumetric moisture content (θ_v, %) within a soil depth range of 0.0 – 0.3 m below ground level (b.g.l) and 0.15 m away from the tree bole on the downslope side of the stem. Mean profile θ_v was 5.1± 2.3%. Thirty-six hours after spraying the dye solution, we dug a 2.0 x 1.0 m trench downslope from each tree 0.3 m away from the tree bole (Fig. 2). The wall of each trench was smoothed with a knife prior to mapping the dyed areas and the root profiles onto a 1.0 m x 0.5 m gridded acetate sheet (Böhm, 1979). The area of dyed soil was quantified at 0.1 m intervals along the soil profile by examining the proportion inside each grid square that was stained (Nespoulous et al., 2019). The cross-sectional area of all roots (*Ar*; mm^2) was quantified at the same soil depth intervals (Gonzalez-Ollauri and Mickovski (2016); Eqs. 1 and 2 (Table 1)), once sycamore roots had been identified (Reward et al., 2012).

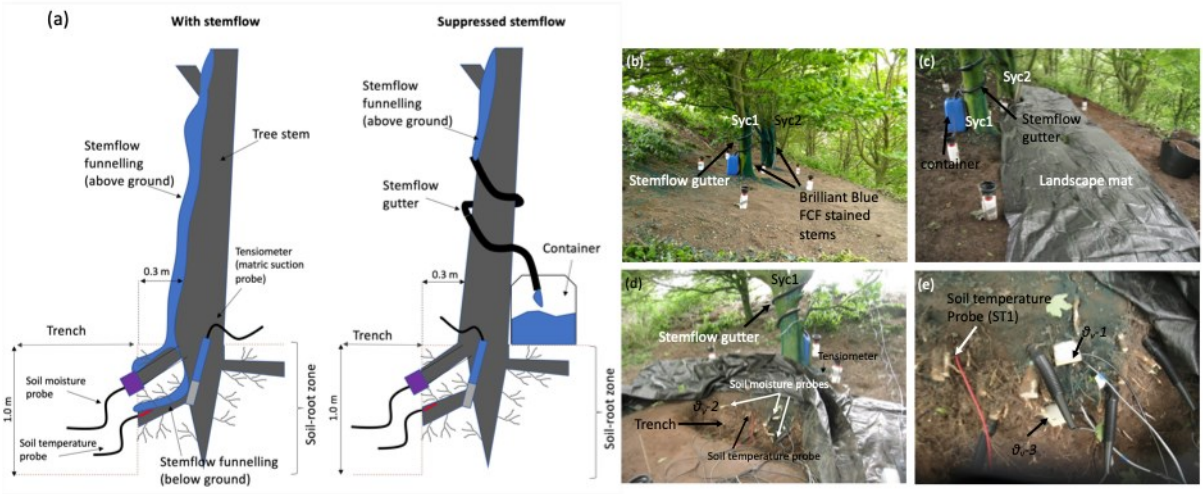

Figure 2. (a) Illustration showing the experimental setup deployed onsite to study soil-water dynamics with stemflow (Syc2) and without stemflow (Syc1); (b) Brilliant Blue FCF was sprayed on the stem of Syc1 and Syc2 prior to suppressing stemflow in Syc1 with a gutter. Most of the dye solution infiltrated the soil next to the tree bole; (c-e) trenches were dug to observe the distribution of Brilliant Blue FCF belowground and to install sensors monitoring soil-water dynamics at the root-soil interface. The trenches were covered with a landscape mat to avoid interference with dripfall and throughfall, θ_v*-1*, θ_v*-2*, and θ_v*-3* indicate the soil moisture probes used under Syc1 (see Table 2). More images from the experimental set up are shown in supplementary material.

191

192

193 *Table 1.* List of equations used in this study. †variable scaled with the projected canopy-crown area (C_A, m^2). ¥Equations implemented in the data mining workflow (see Section 2.6).

Definition	Equation	No	Parameters	Units	Source
Cross-sectional area of roots	$Ar = \pi.(\Sigma d/2)^2$	Eq.(1)	*Ar:* Cross-sectional area of all roots at a given soil depth *d:* root diameter	mm^2 mm	Gonzalez-Ollauri and Mickovski (2016)
Vertical root distribution	$Ar(z) = Aro.e^{-z/b}$	Eq.(2)	*Ar(z)*: cross-sectional area of all roots along the soil profile *Aro*: cross-sectional area of the stump *b*: mean rooting depth *z:* soil depth	mm^2 mm^2 mm mm	Preti et al. (2010) Gonzalez-Ollauri and Mickovski (2016)
Stemflow yield	$Sy = a + b.Pg$	Eq.(3)	*Sy*: stemflow yield *Pg*: incident rainfall *a*: intercept *b*: slope	L mm	Deguchi et al. (2006)
Stemflow funnelling ratio	$SFR = \frac{Sy}{Pg\ .\ DBH}$	Eq.(4)	*DBH*: stem diameter at breast height (i.e. 1.4 m from the ground level)	m^2	Herwitz (1986)
¥Stemflow yield and tree architecture	$Sy = f(Pg, Ht, C_A, DBH, c, LAI, S_L, PBr, SBr, mxBra,$ $+mnBra, nL, L_{BM}, Br_{BM}, C_{BM})$	Eq.(5)	*Ht*: tree height C_A: projected canopy-crown area *DBH*: diameter at breast height (i.e. 1.4 m from the ground level) *c*: canopy cover fraction *LAI*: leaf area index S_L: stem lean from the vertical axis measured at the ground level †*PBr*: number of primary branches (i.e. developing from the main stem; Fig. 1a) †*SBr*: number of secondary branches (i.e. borne on the primary branches; Fig. 1a) *mxBra*: maximum branching angle from the horizontal axis *mnBra*: mean branch angle from the horizontal axis †*nL*: leaf count †L_{BM}: leaf biomass †Br_{BM}: total branch biomass (i.e. primary and secondary branch biomass) †C_{BM}: crown biomass	m m^2 m % m^2 m^{-2} ° m^{-2} m^{-2} ° ° m^{-2} $g\ m^{-2}$ $g\ m^{-2}$ $g\ m^{-2}$	This study
¥Soil temperature	$ST = f(Pg, Sy, Ta)$	Eq.(6)	*ST*: soil temperature measured from June to October, 2018 *Pg*: incident rainfall (i.e. rainfall that reaches the soil without vegetation) measured from June to October, 2018 *Sy*: stemflow yield measured from June to October, 2018 *Ta*: air temperature measured from June to October, 2018	° mm mL °	This study
¥Soil moisture	$\theta v = f(Pg, Sy, Ta)$	Eq.(7)	θ_v: soil moisture measured from June to October, 2018	/1	This study

¥Soil matric suction	$\psi = f(Pg, Sy, Ta)$	Eq.(8)	Ψ: matric suction measured from July to August, 2018	kPa	This study

194

195 2.4. Quantification of stemflow and funnelling ratio

196

197 Stemflow was suppressed for two of the three sycamore individuals (Syc1 and Syc3, Figs.
198 2a,b), so that the influence of aboveground tree architecture on double-funnelling (Section
199 2.6; Fig. 3a) could be quantified. Suppressing stemflow also allowed us to determine
200 indirectly its contribution to soil-water dynamics (Fig. 3a). This suppression was achieved by
201 sealing one stemflow gutter (32 mm diameter, corrugated vinyl tube, with a third of its
202 perimeter cut off to enable the collection of stemflow), starting at a height of 1.7 m up the
203 tree stem, and revolving one and a half times around the stem (Figs. 2a,b; Gonzalez-Ollauri
204 and Mickovski, 2017a). Each stemflow gutter terminated in a 25 l opaque plastic container
205 where stemflow water was collected and stored until measurement (Fig. 2a). The amount of
206 stemflow collected was measured with a graduated cylinder on a rainfall event basis from
207 July to October, 2018. On 21/06/2018, and after trenches had been dug (Section 2.3), we
208 cleared out the understory vegetation, and covered the ground surface below the canopies of
209 Syc1 and Syc2 with a landscape mat. This mat prevented the infiltration of water from
210 dripfall and throughfall (e.g. Zimmermann and Zimmermann, 2014) into the soil but allowed
211 stemflow infiltration under Syc2 (Fig. 2c).

212

213 Stemflow yield was compared against incident rainfall (*Pg*; mm d^{-1}) by fitting linear
214 regression models (Eq. 3, Table 1; Deguchi et al., 2006) in R v3.5.1 (R Core Team, 2018).
215 Rainfall and air temperature time series were retrieved with a 1-minute resolution from a
216 Davis Vantage Pro2 meteorological station located *in situ* and away from the canopy's
217 influence (voor de Poorte, 2018; Fig. S1a). We monitored 35 rainfall events in total, with an
218 event defined as having a minimum depth of 0.4 mm and being separated by at least 2 hours
219 without rainfall. We strived to measure stemflow volume 2h after rainfall or the following
220 morning when the former was not possible. When more than one rainfall event occurred
221 before we could measure stemflow (seven events in total), we assumed a linear relationship
222 between rainfall and stemflow, and we proceeded as follows: (i) we measured the total
223 stemflow volume collected in the container; (ii) we then discretised rainfall events by
224 aggregating the 1 minute rainfall time steps into hourly steps; (iii) we subset and pooled
225 consecutive time steps with rainfall depths above 0.4 mm; (iv) we summed up the rainfall
226 depth for the pool of unmonitored events; (v) we estimated the volume ratio for each event
227 considering the total rainfall volume, and finally, (vi) we applied this ratio to the total

stemflow volume collected in the container. Once stemflow yield was known, the stemflow funnelling ratio (*SFR*) was calculated at the individual level as indicated in Eq. 4 (Table 1; Herwitz, 1986).

2.5. Influence of stemflow and its suppression on soil-water dynamics

After trenches had been dug for the observation of dyed water originating from stemflow (Section 2.3), we monitored soil-water dynamics under both stemflow (Syc2) and suppressed stemflow (Syc1). We also monitored soil-water dynamics in zones with and without signs of double-funnelling (i.e. with and without blue staining) (Figs. 2d,e). To do so, we measured soil temperature (*ST*, °C), soil volumetric moisture content (θ_v, /1), and soil matric suction (ψ, kPa) using automatic sensors during the growing season of 2018 (i.e. late June – early October, 2018).

Every sensor was deployed at the interface between roots larger than 5 mm in diameter and soil (Fig. 2a) at locations noted in Table 2. Soil moisture content was monitored with seven time-domain reflectometry sensors (TDR; CS616 – Campbell Scientific, UK) installed at different soil depths (Table 2) in the excavated trenches (Figs. 2c, d). Soil temperature was monitored in the excavated trenches under stemflow and suppressed stemflow by installing one temperature probe (T107 – Campbell Scientific, UK) per trench and in areas that had been stained with dye (Table 2; Figs. 2c,d). Soil matric suction was monitored with two field tensiometers/piezometers (T4 – UMS GmbH, Germany) installed vertically within the soil-root zone (i.e. 0-500 mm beneath the soil surface; Gonzalez-Ollauri and Mickovski, 2017a; Tardio et al., 2016) and, at 0.1 m from the downslope side of the tree boles of Syc1 and Syc2. All sensors were wired to a solar powered CR-1000 data logger (Campbell Scientific, UK), that collected records for *ST*, θ_v, and ψ at 15 minute time steps. To test the operational capacity of the instrumental setup, we undertook four stemflow simulation events at the onset of the monitoring period (event 1 on 28/06/2018; event 2 on 03/07/2018; event 3 on 04/07/2018; and event 4 on 09/07/2018). Each stemflow simulation event consisted of spraying 20 L of tap water at a height of 1.7 m over the downslope side of the stem of Syc1 and Syc2 using a backpack sprayer for 35 minutes (i.e. rainfall intensity of 45.7 mm h^{-1}). The results from these simulations were analysed together with the records derived from real stemflow events occurring during the monitoring period.

Table 2. Sensor type and location in stained/unstained soil under trees with stemflow or where stemflow was suppressed. Sensors measure soil temperature (*ST*), soil moisture (θ_v) and matric suction (ψ). Sensor Id refers to the sensor type and number.

Variable	Sensor	Sensor Id	Tree	Treatment	Positioned in zone previously stained with blue dye from stemflow?	Depth (mm)
Soil temperature	T107	*ST1*	Syc1	Suppressed stemflow	Yes	150
	T107	*ST2*	Syc2	Stemflow	Yes	150
Soil moisture	CS616	θ_v*-1*	Syc1	Suppressed stemflow	Yes	100
	CS616	θ_v*-2*	Syc1	Suppressed stemflow	No	100
	CS616	θ_v*-3*	Syc1	Suppressed stemflow	Yes	260
	CS616	θ_v*-4*	Syc2	Stemflow	No	400
	CS616	θ_v*-5*	Syc2	Stemflow	Yes	100
	CS616	θ_v*-6*	Syc2	Stemflow	No	100
	CS616	θ_v*-7*	Syc2	Stemflow	Yes	400
Soil matric suction	T4	ψ*-1*	Syc1	Suppressed stemflow	Yes	300-400
	T4	ψ*-2*	Syc2	Stemflow	Yes	300-400

2.6. Framework description and implementation

We defined a cascade-style, numerical framework that incorporates a data mining workflow to evaluate the relationships between tree architecture, stemflow, and stemflow-derived soil-water dynamics (i.e. soil temperature, volumetric soil moisture content and matric suction, Fig. 3a). The framework was built using the statistical software R v3.5.1 (R Core Team. 2018). Data mining was implemented twice (Figs. 3a-b): (i) to explore the effect of tree architecture on stemflow yield, and (ii) to assess the effect of stemflow yield, rainfall, and air temperature on soil-water dynamics.

The data mining workflow fits 100 boosted regression tree models (BRTs; Breiman et al. 1984) without pruning, using the R package "rpart" (Therneau and Atkinson, 2018). Each BRT was fitted using a training dataset generated through a bootstrapping method with

replacement (Efron, 1979). Accordingly, a dataset containing 70 % of the observations (i.e. the training dataset) was extracted for each model run. The model outcomes were then cross-validated with the remaining 30 % of the data. Model quality was evaluated depending on the value of the coefficient of determination (R^2) and the root mean square error (RMSE), between predicted and observed values, following the least-squares criterion (e.g. Bruce and Bruce, 2017). The best fitted BRT was selected on the basis of its quality and the amount of information carried by the regression tree (i.e. the number of relevant covariates portrayed in the BRT). In addition, the relative influence (*RI*; %; e.g. del Campo et al., 2018) of each covariate on the response variable was examined through the evaluation of the decrease in node impurities (i.e. reduction in mean squared error), produced by splitting each regression tree on a given metric using the R package "caret" (Khun, 2018). The nature of the relationships between response and predictor variables were then evaluated on the basis of partial dependence plots (e.g. Tanaka et al., 2017), retrieved with the R package "pdp" (Greenwell, 2017).

The steps followed to implement the proposed framework (Fig. 3a) are illustrated in Fig. 3b. Firstly, the data mining workflow was implemented to fit stemflow yield BRT models using Eq.5 (Table 1) and the information collected from Syc1 and Syc3. Incident rainfall was included as covariate in the fitting of BRTs (Fig. 3a). The purpose of this was twofold: (i) to enable prediction of stemflow yield under varying incident rainfall, and (ii) to investigate the effect of tree architecture masked by the relationship between incident rainfall and stemflow yield (Deguchi et al., 2006) – i.e. how rainfall events are partitioned into stemflow by an array of steady-state, tree architectural traits at an individual level. Model quality, covariates' *RI*, and relationship between predictors and response variables were then examined as described above (Fig. 3a). Following model cross-validation and best model selection (Fig. 3a), stemflow yield was predicted for Syc2 with the best performing BRT. For this, the measured tree architectural traits in Syc2 and incident rainfall were used as inputs (Fig. 3b).

Subsequently, soil-water BRT models were fitted to the monitored soil-water variables (i.e. *ST*, θ_v, and ψ), using Eqs. 6, 7 and 8, respectively (Table 1). To this end, air temperature, incident rainfall, and predicted stemflow yield were used as inputs for Syc2 (Fig. 3b), while the stemflow yield inputs were assumed to be zero for Syc1 (i.e. tree with suppressed stemflow). Air temperature was included to investigate soil-water dynamics during drying (i.e. in the absence of precipitation), as air temperature and soil-water tend to be tightly

coupled (e.g. Feng and Liu, 2015). Incident rainfall was included to detect soil-water dynamics that were not related to stemflow in the context of this study, e.g. subsurface flow generated away from the canopy's influence, but still reaching the soil-root zone under study (Bogaard, 2001). BRT models were fitted per monitoring sensor (Table 2) and per tree individual where soil-water dynamics were studied (Syc1 and Syc2).

All time series were aggregated into daily time steps prior to fitting the BRT models. Model quality was evaluated using the probability density functions from the pool of R^2 values retrieved from cross-validation (Fig. 3a). The *RI* of the covariates (i.e. air temperature, incident rainfall, and stemflow yield), on soil-water dynamics and the relationship between predictors and response variables were then examined as described above (Fig. 3a).

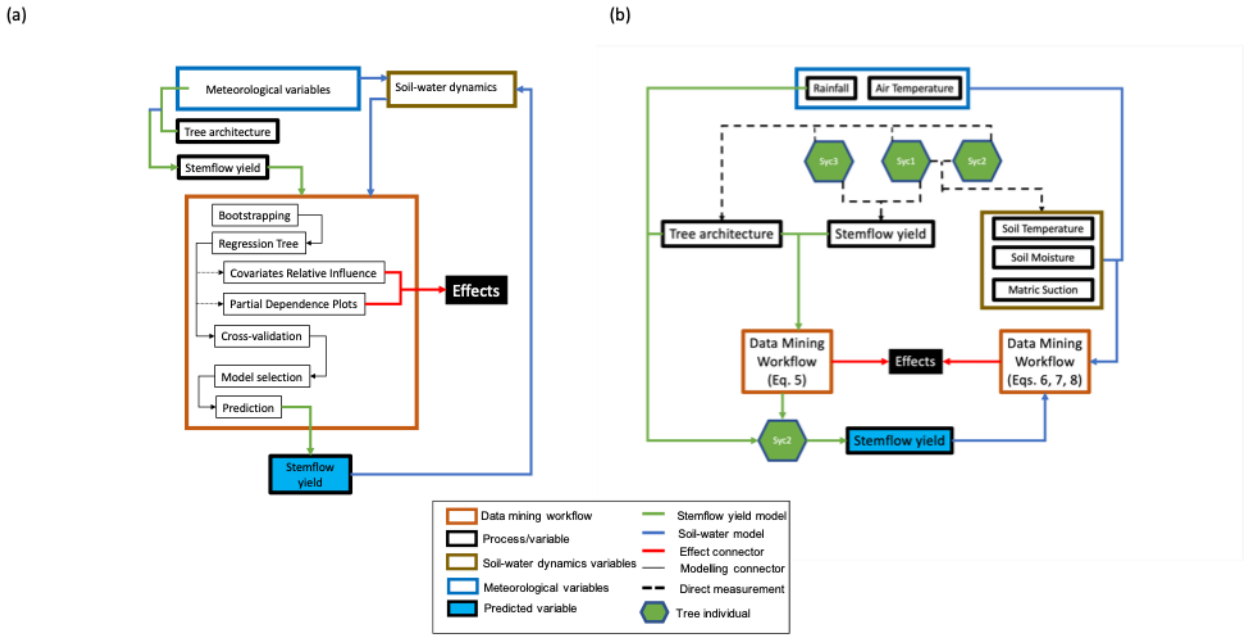

Figure 3. (a) Proposed framework to study the effect of tree architecture on stemflow yield, and the effect of stemflow yield and external meteorological variables (i.e. rainfall and air temperature) on soil-water dynamics, i.e. soil temperature, soil moisture, and matric suction. (b) Flow chart illustrating the implementation of the proposed framework in this study. See online version for colours.

2.7. Statistical analysis

The vertical distribution of tree roots and the soil area affected by double-funnelling were correlated using Pearson's correlation (r) tests. Non-parametric Kruskal-Wallis (χ^2) tests

were then performed to determine differences in stemflow yield between individuals on an event basis. Kruskal-Wallis tests were also used to evaluate differences in daily levels of *ST*, θ_v, and ψ between trees with stemflow and those where stemflow was suppressed. Differences in model quality between the fitted BRTs (i.e. R^2; Section 2.6) as well as differences between covariates' *RI* generated for the 100 BRTs fitted to tree architectural traits and to soil-water dynamics parameters, respectively, were also evaluated with Kruskal-Wallis tests. Stemflow yield was excluded from statistical analyses evaluating differences between covariate's *RI* on *ST*, θ_v, and ψ for Syc1, as stemflow yield was assumed to be zero for this tree (i.e. tree with suppressed stemflow). All statistical tests were performed using the software R v3.5.1 (R Core Team, 2018), at 95% and 99% confidence levels, following normality testing through Shapiro-Wilk tests.

3. Results

3.1. Aboveground tree architectural traits

Sycamore trees had smooth stems with 3 to 5 primary branches inserted above 1.7 m, from which 60 to 80 secondary branches emerged (Table 3). The two individuals on which stemflow yield was quantified (Syc1 and Syc3; Table 3) were similar with regard to *DBH* and C_A (Table 3), but they also had substantial dissimilarities in most of the remaining architectural traits, reflected in differences in stemflow yield (Table 3). Syc3 had greater leaf and branch biomass, with more primary and secondary branches, but exhibited less stem lean (5°) than the other individuals (10° and 19° from the vertical axis). The sycamore individual where stemflow was allowed to yield freely into the soil beneath (Syc2) was larger size in terms of *DBH,* C_A, and *Ht,* and was more inclined, but had less leaves and less inclined branches compared to Syc1 and Syc3 (Table 3).

Table 3. Aboveground architectural traits and total stemflow yield for the monitoring period (July-October, 2018) for the three sycamore individuals. *DBH*: diameter at breast height; C_A: projected canopy-crown area; c: canopy cover fraction; *Ht*: tree height; *LAI*: leaf area index; S_L: stem lean; $mxBr_a$: maximum branch insertion angle; $avBr_a$: mean branch insertion angle; *PBr:* number of primary branches per unit area of canopy-crown; *SBr*: number of secondary branches per unit area of canopy-crown; *nL*: leaf count per unit area of canopy-crown; L_{BM}: leaf biomass per unit area of canopy-crown; Br_{BM}: branch biomass per unit area of canopy crown. * stemflow yield was predicted in Syc2 as shown in Fig. 3b.

Sycamore individual	*DBH* (m)	C_A (m^2)	*c* (%)	*Ht* (m)	*LAI*	S_L (°)	$_{mx}Br_a$ (°)	$_{av}Br_a$ (°)	*PBr* (m^{-2})	*SBr* (m^{-2})	*nL* (m^{-2})	L_{BM} (g m^{-2})	Br_{BM} (g m^{-2})	Total Stemflow yield (mL

														m^{-2})
Syc1	0.37	38.88	93	7.41	5.28	10	55	38	0.08	1.54	499.64	213.60	2557.06	2341.77
Syc2	0.49	53.84	89	11.38	4.53	19	40	28	0.09	1.30	429.53	183.63	2512.81	137.17*
Syc3	0.34	37.34	98	4.06	3.83	5	50	35	0.13	2.11	689.29	294.66	3765.61	3521.61

3.2. Stemflow yield and funnelling ratio

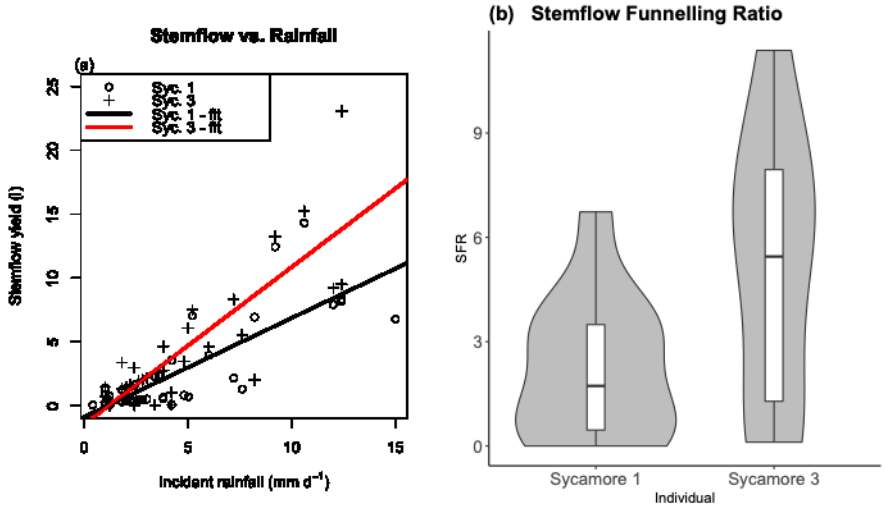

Figure 4. (a) Stemflow yield was significantly higher in sycamore Syc3 ('+' symbol and red line, y=1.23x-1.45, $R^2 = 0.69$, $P < 0.01$) compared to Syc1 (empty circles and black line, y=0.77x-0.88, $R^2 = 0.63$, $P < 0.01$), with respect to incident rainfall (mm d^{-1}); (b) stemflow funnelling ratio (SFR, unitless) for Syc1 and Syc3. The lower edge of the box corresponds to the 25th percentile data point, while the top edge of the box corresponds to the 75th percentile data point. The line within the box represents the median. The grey area around the box shows the probability density of the data at different values. See online version for colours.

Stemflow yield significantly increased with the incident rainfall in both sycamore individuals (Fig. 4a), it being significantly greater in Syc3 when compared to Syc1. The rainfall threshold to yield stemflow was 1.14 mm d^{-1} and 1.18 mm d^{-1} for Syc1 and Syc3, respectively. The total stemflow yield during the monitoring period was 91.05 l and 131.50 l for Syc1 and Syc3, respectively. For both trees and the 35 rainfall events examined, the mean stemflow amount generated per unit projected crown area averaged 1.35 % of the incident rainfall, with a maximum of 3.76 %. Mean stemflow funnelling ratios were above 1.0 in all cases (i.e. more incident rainfall was concentrated around the tree bole than expected had there not been a tree; Fig. 4b) but they did not differ statistically between the two sycamores (χ^2=3.46, df=1, p=0.06). However, the mean stemflow funnelling ratio was substantially higher in Syc3 (5.16±3.91) than in Syc1 (2.23±2.11).

3.3. Double-funnelling and tree root distribution

391

Figure 5. (a) Area within the soil-root zone where subsurface flow had occurred due to double-funnelling and root vertical distribution for sycamores Syc1 (full green circles and dotted line) and Syc2 (full black circles and dotted line). A negative exponential model (lines) was fitted to the measured root area (points) (Gonzalez-Ollauri and Mickovski, 2016). Soil stained with Brilliant Blue FCP dye indicated double-funnelling into soil beneath (b) Syc1 and (c) Syc2. See online version for colours.

392

393 In trees that had been sprayed with dye, zones where subsurface flow had occurred due to
394 double-funnelling were successfully identified in the soil close to the stem (Figs. 5b and c).
395 The dye solution mostly infiltrated into the topmost soil layers, reaching maximum depths of
396 350-400 mm b.g.l (Fig. 5a). Specific zones with signs of preferential flow were also
397 identified, and associated with the presence of thicker roots (Figs. 5b-c). The area of soil
398 wetted by double-funnelling (Fig. 5a) was not significantly different between Syc1 and Syc2
399 (χ^2=0.18, df=1, p=0.68; Fig. 5a). However, we detected a strong positive correlation (r=0.57)
400 between the stained area of soil and vertical root distribution, and both decreased with
401 increasing soil depth (Fig. 5a). The root cross-sectional area (*Ar*) of the two sycamores
402 decreased exponentially with increasing soil depth and had mean rooting depths (i.e. *b*: soil
403 depth at which 95 % of the roots are located; Gonzalez-Ollauri and Mickovski, 2016; Table
404 1) of 258.9 mm and 275.8 mm for Syc1 and Syc2, respectively.

405

406

407 3.4. Influence of stemflow and its suppression on soil-water dynamics
408
409
410
411 3.4.1. Soil temperature
412
413 Daily soil temperature showed a clear response to stemflow (Fig. 6a) in that it was usually
414 significantly higher (χ^2=3143, df=1, p < 0.01) under the tree where stemflow was suppressed.

However, under Syc2 with stemflow, a substantial increase in soil temperature was observed following heavy rainfall (i.e. > 5-10 mm d^{-1}; Fig. 6a) that was not detected in the tree with suppressed stemflow.

3.4.2. Soil moisture

Distinct daily soil moisture (θ_v) peaks were observed under trees with stemflow after heavy rainfall events (i.e. > 5-10 mm d^{-1}) and following stemflow simulations (Fig. 6b). This response was more pronounced in soil where double-funnelling had occurred, but it was not detected when stemflow was suppressed. Despite this, the θ_v time series did not show significant differences between stemflow and suppressed stemflow (χ^2=2.30, df=1, p=0.13), not even between the locations with and without signs of double-funnelling (χ^2=1.89, df=1, p=0.17; Table 2). However, significant differences occurred between soil depths where soil moisture probes were deployed: shallow soil (i.e. 100 mm b.g.l) had significantly higher θ_v compared to deeper soil (i.e. 260 and 400 mm b.g.l; Table 2; χ^2=13.09, df=2, $p < 0.01$; Fig. 6b). We excluded soil moisture records from θ_v-1 (Table 2; Figs. 2c,d), as the moisture probe was dysfunctional (Fig. 6b).

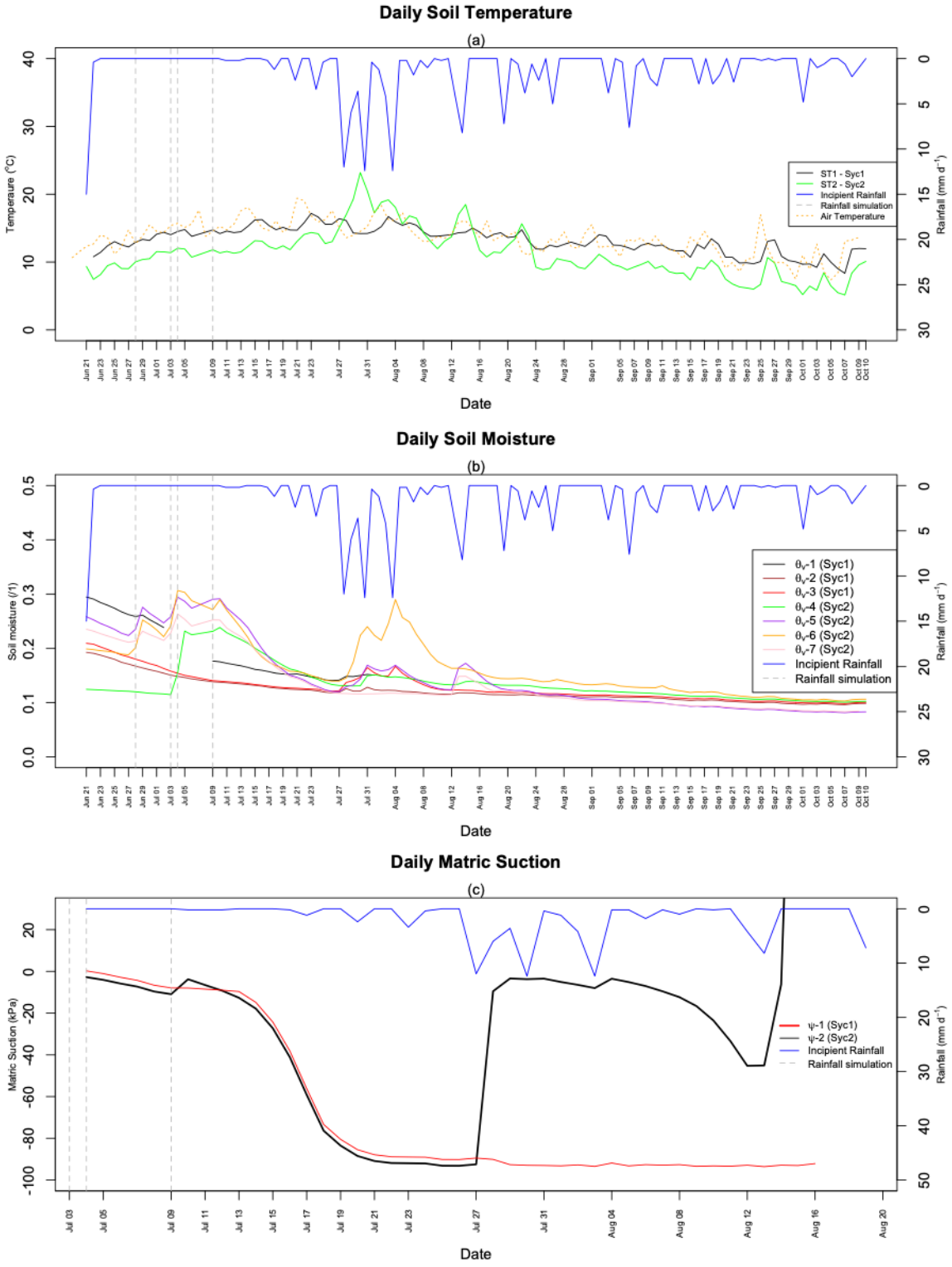

Figure 6. (a) Daily mean soil temperature time series recorded at two points (Table 2) where signs of double-funnelling had occurred under Syc1 (suppressed stemflow) and Syc2 (with stemflow), plotted together with daily mean air temperature and incident daily rainfall data. (b) Daily mean volumetric soil moisture content recorded for Syc1 (suppressed stemflow) and Syc2 (with stemflow), at different areas of the root-soil zone (Table 2), and plotted together with incident rainfall data. (c) Daily mean matric suction recorded at the root-soil zone (Table 2) under Syc1 (suppressed stemflow) and Syc2 (with stemflow). Vertical dot-dash lines indicate stemflow simulation events undertaken after trench excavation (Section 2.5). See online version for colours.

434

435

436 3.4.3. Soil matric suction

437

438 Daily soil matric suction (ψ) responded to stemflow markedly over the monitoring period
439 (Fig. 6c) and increased (i.e. became more negative) in both sycamore individuals under dry
440 conditions (i.e. in the absence of rainfall), until it reached the maximum measurable value
441 possible with the tensiometer (-93 kPa; Fig. 6c). However, ψ decreased sharply following
442 heavy rainfall events (>5 mm d^{-1}) in the sycamore individual that had double-funnelling
443 (Syc2; Fig. 6c). However, Syc1 (i.e. suppressed stemflow) showed no change in ψ (Fig. 6c).
444 The same effect, although of lower magnitude, was observed following stemflow simulations
445 around Syc2 (vertical dot-dash lines in Fig. 6c). As a result, ψ was significantly different
446 between individuals with stemflow, and those where stemflow was suppressed (χ^2=44.40,
447 df=1, p<0.01). At the end of the observation period, ψ in soil beneath Syc2 decreased towards
448 positive values (i.e. positive pore-water pressure; Fig. 6c). We excluded soil matric suction
449 records after 16/08/2018 (Table 2), as the *ψ-2* probe was dysfunctional after this date (Fig.
450 6c).

451

452 3.5. Framework outputs

453

454 3.5.1. Effect of tree architectural traits on stemflow yield

455

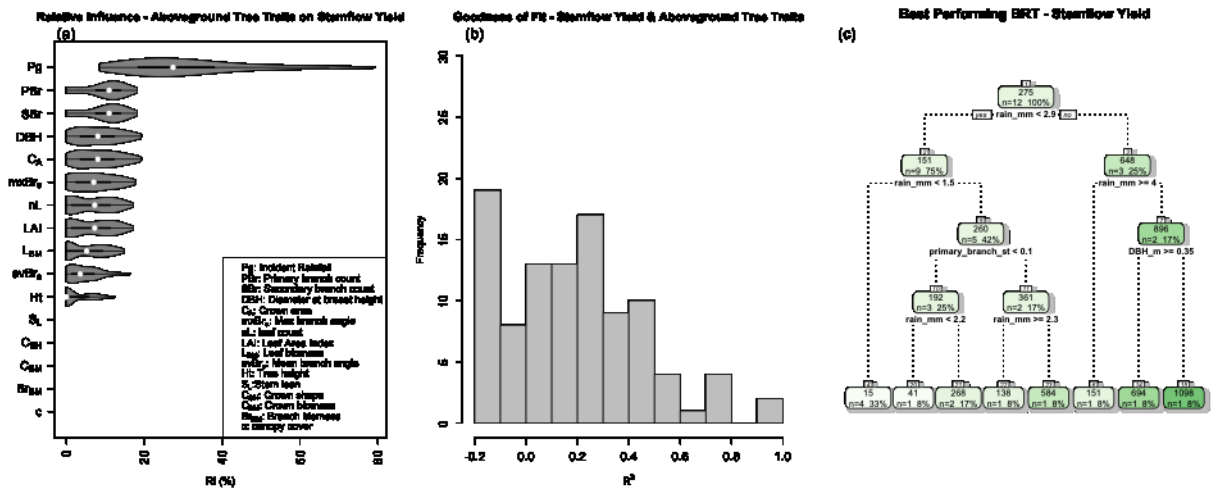

Figure 7. (a) Incident rainfall had the highest relative influence (RI) on stemflow yield for Syc1 and Syc3, followed by several architectural traits related to branch dimensions and leaf cover; the white dot within the box represents the median while the grey area around the box shows the probability density of the data at different values (b) Histogram showing the frequency of coefficients of determination (R^2) for the 100 boosted regression trees fitted between aboveground traits against stemflow yield for sycamores Syc1 and Syc3 (c) Regression tree dendrogram for the best performing BRT model fitted to predict stemflow yield from tree architectural traits and incident rainfall. Each tree leaf (i.e. box) indicates the mean response (i.e. stemflow yield in ml), number, and percentage of observations. The darker the colour shade in the tree leaf, the higher is the mean response.

The relative influence (*RI*) of architectural traits (Fig. 7a) on stemflow yield was significantly different (χ^2=1225, df=15, p<0.01), implying that the measured architectural traits contributed differently to the partition of rainfall into stemflow aboveground. Incident rainfall, which was included as covariate in the BRTs (Section 2.6.1; Fig. 7c), was the most important predictor (*Pg*; 31.48±16.02%; Fig. 7a). Stem lean (S_L), crown shape (C_{SH}), and biomass (C_{BM}), branch biomass (Br_{BM}) and canopy cover fraction (*c*) did not influence the production of stemflow yield (Fig. 7a). In the light of the best performing BRT (Fig. 7c) and partial dependence plots (PDPs; supplementary material Figs. S2a-p), incident rainfall and the number of primary branches were strongly and positively correlated with stemflow yield (Figs. 7c, S2a,f) while a strong, negative correlation was observed between stemflow yield and *DBH* (Figs. 7c, S2b). The PDP between stemflow yield and incident rainfall (Fig. S2a) indicated that there was a rainfall threshold of 3.5 mm d^{-1} for the production of stemflow, in contrast with the thresholds of 1.14 and 1.18 mm d^{-1} observed in Fig. 4a (Section 3.2). Beyond rainfall of 3.5 mm d^{-1}, stemflow yield was the same. The remaining aboveground traits did not show clear correlations with stemflow yield (Figs. 7c, S2), in spite of the observed *RI* (Fig. 7a). The fitted BRTs presented a maximum R^2±RMSE of 0.94±19140, and a mean±SD and mode R^2 of 0.19±0.26 and 0.25, respectively (Fig. 7b).

3.5.2. Effects of stemflow yield, incident rainfall, and air temperature on soil-water dynamics

3.5.2.1. Soil temperature

The BRTs fitted to soil temperature (Eq. 6 - Table 1; Fig. 3) had a high goodness of fit overall (supplementary material Figs. S3a-b; Table 4). The R^2 density function for *ST* (Figs. S3a-b) exhibited negative skewness and a mean value above 0.5 (Table 4). Model quality was significantly higher (χ^2=37.94, df=1, p<0.01) under Syc1 with suppressed stemflow (Fig. S2a) compared to Syc2 (with stemflow, Fig. S3b). The assessment of the variables' *RI* for all the BRTs fitted to soil temperature (Fig. 8a-b) suggested that air temperature was the most important covariate for predicting soil temperature (Fig. 6a), which was significantly more important than rainfall and stemflow for Syc2 (χ^2=92.55, df=2, p<0.01). However, air temperature and rainfall were equally important for predicting *ST* when stemflow was

suppressed (χ^2=3.67, df=1, p=0.05). The influence of incident rainfall and air temperature on soil temperature was corroborated in the partial dependence plots for Syc2 (supplementary material Figs. S4a-c), whereas the effect of stemflow was unclear (Fig. S4b). For Syc1, however, the effect of rainfall on soil temperature was uncertain (Fig. S4a), while air temperature had a more constant influence on soil temperature than that observed beneath Syc2 (Fig. S4c).

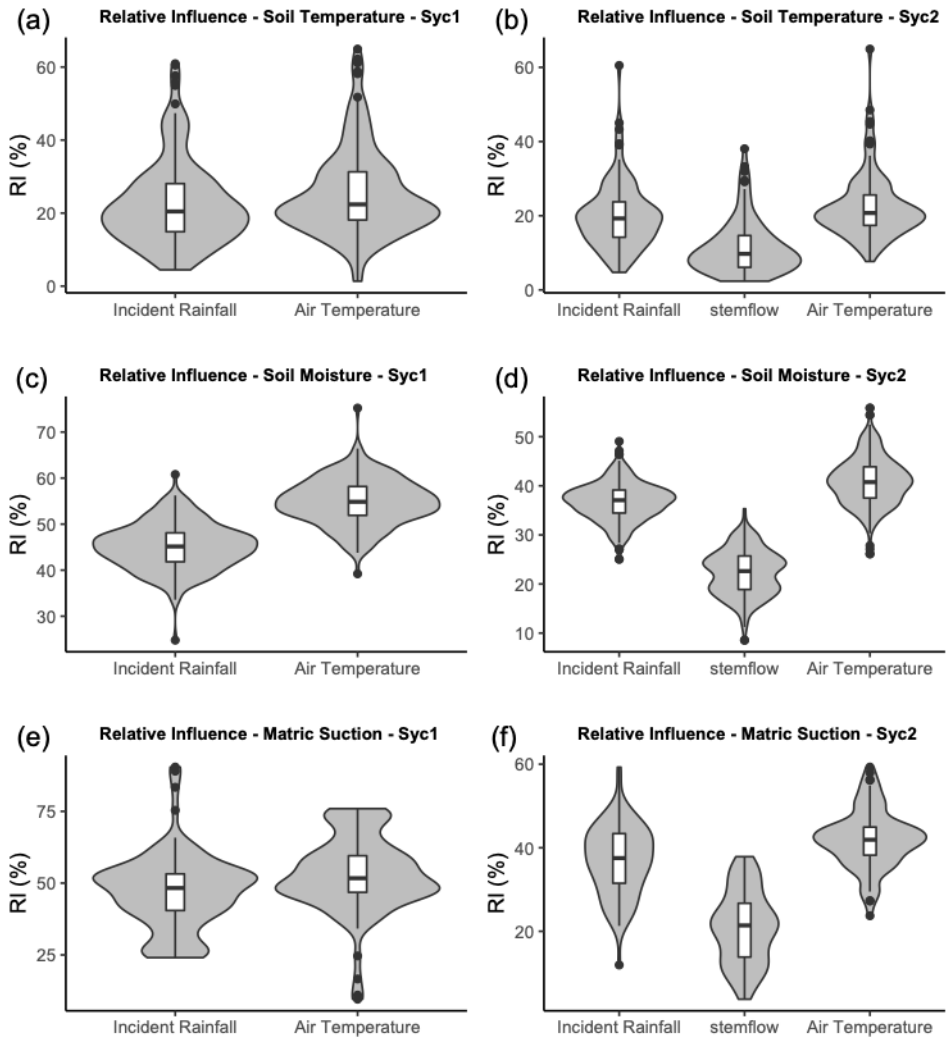

Figure 8. Relative influence (*RI*) of stemflow yield, incident rainfall and air temperature on soil-water dynamics for sycamores Syc1 (suppressed stemflow) and Syc2 (with stemflow) (a-b) soil temperature (c-d) soil moisture (e-f) matric suction. The lower edge of the box corresponds to the 25th percentile data point, while the top edge of the box corresponds to the 75th percentile data point. The line within the box represents the median. The grey area around the box shows the probability density of the data at different values.

520
521
522 3.5.2.2. Soil moisture
523
524 The BRTs fitted to soil moisture (θ_v ; Eq. 7 - Table 1; Fig. 3) had a satisfactory goodness of
525 fit in almost all cases under Syc1, where stemflow was suppressed (supplementary material
526 Figs. S3c-h; Table 4). The coefficient of determination (R^2) was also significantly higher
527 (χ^2=194.31, df=1, p<0.01) under Syc1 (Figs. S3c-d) compared to Syc2 (Figs. S3e-h). The
528 assessment of the variables' *RI* for all the BRTs fitted to θ_v (Figs. 8c-d) suggested that air
529 temperature was the most important predictor for soil moisture (Fig. 6b), even more so than
530 rainfall and stemflow (Syc1: χ^2=205.9, df=1, p<0.01; Syc2: χ^2=851.6, df=2, p<0.01).
531 However and, on the basis of the PDPs (supplementary material Fig. S4), only air
532 temperatures ranging between 10 and 11^o C seemed to produce a minor, yet consistent,
533 response on soil moisture (Fig. S4f). The PDPs also showed that the nature of the relationship
534 between rainfall and air temperature with θ_v was unclear for both sycamore individuals (Figs.
535 S4a-f). The same issue was observed between stemflow yield and soil moisture (Fig. S4e).
536
537 3.5.2.3. Soil matric suction
538
539 The BRTs fitted to soil matric suction (ψ ; Eq. 8 - Table 1; Fig. 3) exhibited, in general, a
540 poor goodness of fit (supplementary material Figs. S3i-j; Table 4). No significant differences
541 occurred between the models fitted under Syc1 (suppressed stemflow) and Syc2 (with
542 stemflow, χ^2=0.14, df=1, p=0.71). The assessment of the variables' *RI* for all the BRTs fitted
543 to ψ (Figs. 7e-f) suggested that air temperature was the most important predictor (Fig. 8c),
544 and was significantly more important than rainfall and stemflow (Syc1: χ^2=10.54, df=1,
545 p<0.01; Syc2: χ^2=167.2, df=2, p<0.01). On the basis of the PDPs (supplementary material
546 Figs. S4j-l), the influence of rainfall and air temperature on matric suction appeared constant
547 for Syc1. However, these variables had a cyclical effect on matric suction for Syc2 (Figs.
548 S4j-l). The PDPs for stemflow yield showed a negative relationship with matric suction in
549 Syc2, i.e. higher stemflow yields led to lower matric suction (Fig. S4k).
550

Table 4. Summary from the cross-validation process (Fig. 2) for the 100 boosted regression trees fitted between meteorological variables and soil-water dynamics (Table 1) for the sycamores Syc1 (suppressed stemflow) and Syc2 (with stemflow). *ST*: soil temperature; θ_v : soil moisture; ψ: matric suction; R^2: coefficient of determination; RMSE: root mean square error; SD: standard deviation.

Variable	Tree	Probe	R^2			Skewness	Kurtosis	SD
			max±RMSE[†]	mean	mode			
Soil temperature	Syc1	ST1	0.95±0.50	0.71	0.79	-1.34	4.96	0.19
	Syc2	ST2	0.94±2.24	0.49	0.71	-0.27	2.08	0.26
Soil moisture	Syc1	θ_v - 2	0.94±0.00	0.39	0.38	0.66	-0.17	2.04
		θ_v - 3	0.84±0.01	0.35	0.38	0.38	-0.12	1.72
	Syc2	θ_v - 4	0.77±0.02	0.18	0.13	0.55	0.52	2.11
		θ_v - 5	0.80±0.02	0.19	0.18	-0.14	0.38	2.38
		θ_v - 6	0.83±0.02	0.17	0.11	-0.14	0.65	2.29
		θ_v - 7	0.60±0.03	0.04	-0.02	-0.14	1.06	3.32
Matric suction	Syc1	ψ - 1	0.99±16.92	0.04	-0.22	1.60	5.69	0.30
	Syc2	ψ - 2	0.95±72.71	0.08	-0.33	0.91	2.55	038

4. Discussion

4.1.Stemflow funnelling above ground

Through our novel framework, we showed that relationships existed between stemflow yield and aboveground tree architecture (Figs. 7a-c). In particular, we demonstrated that a thin trunk and small crown increased stemflow yield and funnelling. Our results also showed that stemflow yield was related to the geometry of the tree's crown, in agreement with Levia and Frost, (2003), Levia et al., (2015) and Yuan et al., (2017). More numerous and steeply angled branches, together with a larger surface area, also increased stemflow production, as found by Levia et al., (2015). However, whilst stemflow yield has been found to be negatively correlated with leaf number (Levia and Frost, 2003; Levia et al., 2015), we showed that more leaves actually increased stemflow (Table 3). This result, which relied on a very small sample size, suggests that leaves could deflect part of the intercepted rainfall towards the woody parts of the canopy, thus contributing to stemflow yield (e.g. Martinez-Meza and Whitford, 1996; Deguchi et al., 2006; Liang et al., 2009; Yuan et al., 2017).

Stemflow yield in sycamores fell within commonly reported values for other woody species across biomes (e.g. Carlyle-Moses et al., 2018) and incident rainfall was the most influential

577 variable affecting stemflow yield (Yuan et al., 2017). We detected a minimum rainfall
578 threshold of 1.14 mm d^{-1} required to trigger stemflow (Fig. 4a), and a maximum threshold of
579 3.5 mm d^{-1}, beyond which stemflow yield was constant (supplementary material Fig. S3a).
580
581 Nevertheless, the number of individuals investigated in our study was low, and a wider
582 diversity of tree sizes and architectural traits (e.g. leaf shape and angle of insertion on host
583 branch or bark topography) need examining, so that the model fits between stemflow yield
584 and aboveground architectural traits can be improved. A variety of tree morphologies would
585 also help us to better understand the influence of crown architectural traits on stemflow yield,
586 that we could not disentangle in our study (Figs. 7c, S2). However, our framework was robust
587 enough to account for some of the variability in the linear relationship between stemflow
588 yield and incident rainfall (Figs. 4a, 7a, 7c, S2; Deguchi et al., 2006). Including rainfall as a
589 covariate in the BRTs (Fig. 7c) was useful to gain insights into how rainfall events can be
590 partitioned into stemflow by an array of tree architectural traits at the individual level, and
591 also the hydrological boundaries at which this happens.
592
593 The poor BRT fits possibly underline the difficulty of capturing how stemflow is affected by
594 a complex canopy structure (Levia et al., 2015), but a larger tree sample would help to reduce
595 uncertainty. Reliable information about how tree architecture distributes precipitation within
596 the crown to produce stemflow will be especially useful for urban foresters who need to
597 manage stormwater flow around trees that require regular pruning. The type of pruning
598 performed could actually alter the quantity of rainfall that reaches the soil, as well as its
599 transfer belowground (del Campo et al., 2014).
600
601
602 4.2.Double-funnelling
603
604 An effective concentration of incident rainfall occurred around the tree bole and in the
605 uppermost soil layers, as the stemflow funnelling ratio was > 1 (Carlyle-Moses et al., 2018).
606 Subsurface flow occurred mainly as matrix flow (Schwärzel et al., 2012; Spencer and van
607 Meerveld, 2016), with some preferential flow observed along coarse woody roots. The dense
608 root system in the topsoil, that was comprised chiefly of thin roots (i.e. diameter < 3 mm),
609 was significantly and positively correlated to double-funnelling. Coarse woody roots visible
610 on the soil surface next to the tree bole may have acted as small dams, causing stemflow to

611 pond locally and facilitating its infiltration as matrix flow (Mein and Larson, 1973). Ponding
612 could have also been fostered by the hydrophobicity of soil organic matter (Spencer and van
613 Meerveld, 2016), or a higher proportion of silt at the soil surface (unpublished data; Lu and
614 Likos, 2004). The low soil moisture content that we observed, likely reduced the extent of
615 stemflow-derived surface runoff (Liu et al., 2019), that was only noted next to the tree stems
616 (Fig. 2b). Although some preferential flow was observed (Figs. 5b-c), it would be useful to
617 test whether double-funnelling changes from matrix to preferential flow or to surface runoff
618 under different soil hydrological regimes and under different stemflow rates.
619
620 Double-funnelling had a clear impact on soil temperature and moisture (Figs. 6a-b) with both
621 variables increasing rapidly after heavy rainfall events (i.e. > 5 mm day^{-1} in Syc2). The
622 arrival of water to specific patches of soil, together with peaks in soil temperature could be
623 due to enhanced matrix and preferential flow, and the subsequent increase in microbial
624 activity and respiration (McClain et al., 2003; Kuryakov and Blagodatskaya, 2015) related to
625 the transport of water and nutrients from the canopy to the soil through stemflow (e.g.
626 Germer et al., 2012). Still, further work is required to quantify the effects of double-
627 funnelling on soil respiration fluxes along with the activity of soil microbial communities
628 (e.g. Rosier et al., 2016).
629
630 Soil matric suction was significantly modified in response to double-funnelling (Fig. 6c).
631 Between July and August, we observed two clearly defined wetting fronts that only occurred
632 in the soil-root zone under Syc2, suggesting that stemflow can lead to soil matric suction
633 depletion (Liang et al., 2011). In addition, the positive pore-water pressures that developed
634 under Syc2 after the second recorded wetting front were indicative of the formation of a
635 perched water table at the location where the tensiometer was installed (Germer, 2013). The
636 decrease in soil matric suction that we observed can drastically reduce the mechanical
637 strength of plant-soil composite materials (Vanapalli et al., 1996; Gonzalez-Ollauri and
638 Mickovski, 2017b), thus diminishing the mechanical reinforcement provided by the root
639 system in vegetated slopes (Gonzalez-Ollauri and Mickovski, 2016, 2017b, 2017c). It is not
640 yet known to what extent double-funnelling can alter soil hydrological regimes so that soil
641 slippage and landslides could occur. To prevent such potential occurrences, it is necessary to
642 make a choice on planting tree species based not only on mechanical and hydrological traits,
643 but also taking into account aerial architecture and its potential impact on stemflow.
644

4.3. Effects of stemflow yield, incident rainfall and air temperature on soil-water dynamics

Our framework was useful for detecting effects of stemflow yield and meteorological variables on soil-water dynamics. Air temperature was shown to be the most influential meteorological variable (Fig. 8) and its strong positive correlation with soil temperature could have obscured the effects of rainfall and stemflow yield as predictors of soil temperature. During the summer months, the temperature-dependent, atmospheric demand for water acted as the driver regulating the soil water balance (e.g. Allen et al., 1998; Novick et al., 2016) and hence the dynamics of soil moisture and matric suction in the soil-root zone. However, the effect of rainfall on soil temperature recorded for Syc2, suggested that double-funnelling quickly brought rainfall into the root-soil matrix, and warmed the soil by triggering biogeochemical reactions (Wang et al., 2015; Lloyd and Taylor, 1994; Schindlbacher et al., 2011). In the tree with suppressed stemflow, the effect of rainfall on soil-water dynamics could be related to subsurface flow originated beyond the studied plot, based on the analysis of time lags between rainfall and soil-water dynamics (e.g. supplementary material – Fig. S5; Bogaard, 2001; Bestland et al., 2009).

Surprisingly, stemflow yield was the least important covariate influencing soil-water dynamics in Syc2. The strong correlation between rainfall and stemflow (Figs. 4a, 7a, S2a) may have obscured the relationship with stemflow in the BRTs (model covariates should be independent from each other, Bruce and Bruce, 2017). However, in our study, there were limitations to experimental design because stemflow yield was not directly measured for Syc2, but was predicted for Syc2 using BRTs fitted to a small dataset. Furthermore, Syc2 had substantial architectural differences with respect to the individuals used to fit stemflow yield BRT models (Table 3), which likely led to the poor BRT fits (Fig. S3). Therefore, to clarify the effect of stemflow on soil-water dynamics, it is essential to quantify stemflow yield for a larger sample and longer periods, using flow meters or tipping bucket gauges (e.g. Levia et al., 2010; Spencer and van Meerveld, 2016; del Campo et al., 2018) before allowing stemflow to funnel belowground.

Some limitations occurred when using BRTs, in particular, when we evaluated the relationships between predictors and response variables in the partial dependence plots (PDPs; supplementary material Figs. S2, S4). The discretisation of the response variables by

679 BRTs only enabled us to observe weak predictor-response interactions in the PDPs, as
680 opposed to the array of effects discussed for the time series records (Section 4.2; Fig. 6) as
681 well as for the relationships between architectural traits and stemflow yield (Section 4.1). To
682 circumvent this issue, we encourage the incorporation of alternative statistical models able to
683 generate continuous outputs (e.g. random forest; Breiman, 2001) in future versions of our
684 framework.
685
686 5. Conclusion
687
688 We demonstrated how a novel numerical framework and experimental approach can be used
689 to examine the effect of tree aboveground architecture on stemflow yield and its influence on
690 soil-water dynamics. In the light of our observations and findings, it can be concluded that:
691
692 - The number of branches, their insertion angle, leaf number, and stem basal diameter
693 influenced stemflow yield within specific rainfall thresholds.
694 - Funnelling of stemflow beneath the soil surface occurred as matrix flow and was
695 significantly and positively correlated with the vertical root distribution.
696 - Soil-water dynamics were distinctly different with and without stemflow.
697 - Soil matric suction was negatively affected by stemflow yield, but air temperature
698 was the most influential covariate affecting soil-water dynamics likely due to its
699 strong correlation to evapotranspiration during the summer season.
700 - The discretisation of the response variables by boosted regression trees only enabled
701 us to observe weak predictor-response interactions, as opposed to the array of effects
702 observed in this study.

703 In spite of the study limitations discussed above, such as small sample size and differences
704 between individuals, the proposed framework and experimental approach provide a good
705 basis for future research contributing to our knowledge of how stemflow generated
706 aboveground triggers major responses in soil-water dynamics belowground.

707 Acknowledgment
708

709 The help and support from the Catterline Braes Action Group (CBAG) is greatly
710 acknowledged. Special thanks to Pieter voor de Porte for kindly supplying meteorological

711 records. The help of summer students funded by Erasmus +, Marjorie Pellet and Florian
712 Bourgerie, is deeply appreciated. The authors want to thank Mr Angus Jacobson & Family
713 for site access. We also acknowledge the useful comments and suggestions from the two
714 anonymous referees that helped us to enhance this manuscript. This research project was
715 funded by the BEAM Research Centre of the Glasgow Caledonian University (E0019833 –
716 Prof. Rohinton Emmanuel). Prof. Mickovski's contribution was funded by Erasmus + project
717 ECOMED (575796-EPP-1-2016-ES-EPPKA2-KA).

718 6. References

719

720 Alexander, H., Arthur, M., 2010. Implications of a predicted shift from upland oaks to red
721 maple on forest hydrology and nutrient availability. Can. J. For. Res. 40(4), 716-726
722 Allen, R. Pereira, L., Raes, D., Smith, M., 1998. Crop evapotranspiration guidelines for
723 computing crop water requirements. FAO Irrigation and drainage paper No 56.
724 Barthélémy, D., Caraglio, Y., 2017. Plant Architecture: A Dynamic, Multilevel and
725 Comprehensive Approach to Plant Form, Structure and Ontogeny. Annals of Botany, 99,
726 375-407.
727 Bestland, E. Milgate1, S., Chittleborough, D., VanLeeuwen, J., Pichler, M., Soloninka, L.,
728 2009. The significance and lag-time of deep through flow: an example from a small,
729 ephemeral catchment with contrasting soil types in the Adelaide Hills, South Australia.
730 Hydrol. Earth Syst. Sci., 13, 1201–1214
731 Bialkowski, R., Buttle, J. M., 2015. Stemflow and throughfall contributions to soil water
732 recharge under trees with differing branch architectures. Hydrol. Process., 29, 4069-4082.
733 Blozan, W., 2008. Tree measuring guidelines of the eastern native tree society. Bull. East.
734 Native Tree Soc. 1 (1), 3–10.
735 Böhm, W., 1979. Methods of Studying Root Systems. Springer Verlag, Berlin.
736 Bogaard, T., 2001. Analysis of hydrological processes in unstable clayey slopes.
737 Nederlandse, Geografische Studies
738 Breiman L, Freidman J, Olshen R, Stone C (1984) *Classification and regression trees*.
739 Wadsworth, Belmont, CA.
740 Breiman, L., 2001. Random forests. Mach. Learn. 45, 5–32.
741 Bruce, P., Bruce, A., 2017. Practical statistics for data scientists. O'Reilly, Sebastopol, CA.

742 Carlyle-Moses, D. E., Iida, S., Germer, S., Llorens, P., Michalzik, B., Nanko, K., Tischer, A.,
743 Levia, D. F., 2018. Expressing stemflow commensurate with its ecohydrological importance.
744 Advances in Water Resources, 121, 472-479.
745 Carlyle-Moses, D. E., Price, A. G., 2006. Growing-season stemflow production within a
746 deciduous forest of southern Ontario. Hydrol. Process., 20, 3651-3663.
747 Côté, J. F., Fournier, R. A., Egli, R., 2011. An architectural model of trees to estimate forest
748 structural attributes using terrestrial LiDAR. Environmental Modelling and Software, 26,
749 761-777.
750 Deguchi, A., Hattori, S., Park, H., 2006. The influence of seasonal changes in canopy
751 structure on interception loss: application of the revised Gash model. J. Hydrol. 318, 80–102.
752 del Campo, A. D., Fernandes, T. J. G., Molina, A. J., 2014. Hydrology-oriented (adaptive)
753 silviculture in semiarid pine plantation: How much can be modified the water cycle through
754 forest management? Eur. J. Forest. Res., 133(5), 879-984.
755 del Campo, A. D., Gonzalez-Sanchis, M., Lidon, A., Ceacero, C. J., Garcia-Prats, A., 2018.
756 Rainfall partitioning after thinning in two low-biomass semiarid forests: Impact of
757 meteorological variables and forest structure on the effectiveness of water-oriented
758 treatments. J. Hydrol., 565, 74-86.
759 Efron, B., 1979. Bootstrap methods: another look at the Jackknife. Ann. Stat. 1, 1–26.
760 Feng, H., Liu, Y., 2015. Combined effects of precipitation and air temperature on soil
761 moisture in different land covers in a humid basin. J. Hydrol., 531(3), 1129-1140.
762 Germer, S., 2013. Development of near-surface perched water tables during natural and
763 artificial stemflow generation by babassu palms. J. Hydrol., 507, 262-272.
764 Germer, S., Werther, L., Elsenbeer, H., 2010. Have we underestimated stemflow? Lessons
765 from an open tropical forest. J. Hydrol., 395(3-4), 169-179.
766 Germer, S., Zimmermmann, A., Neill, C., Krusche, A. V., Elsenbeer, H., 2012.
767 Disproportionate single-species contribution to canopy-soil nutrient flux in an Amazonian
768 rainforest. For. Ecol. Manage., 267, 40-49.
769 Gonzalez-Ollauri, A., Mickovski, S.B., 2016. Using the root spread information of pioneer
770 plants to quantify their mitigation potential against shallow landslides and erosion. Ecol. Eng.
771 95, 302–315.
772 Gonzalez-Ollauri, A., Mickovski, S.B., 2017a. Hydrological effect of vegetation against
773 rainfall-induced landslides. J. Hydrol. 549, 374–387.
774 Gonzalez-Ollauri, A., Mickovski, S.B., 2017b. Plant-soil reinforcement response under
775 different soil hydrological regimes. Geoderma 285, 141–150.

776 Gonzalez-Ollauri, A., Mickovski, S.B., 2017c. Plant-Best: A novel plant selection tool for
777 slope protection. Ecol. Eng., 106, 154-173.
778 Gonzalez-Ollauri, A., Mickovski, S.B., 2017d. Shallow landslides as drivers for slope
779 ecosystem evolution and biophysical diversity. Landslides, 14(5), 1699-1714.
780 Greenwell, B. M., 2017. pdp: An R Package for Constructing Partial Dependence Plots. The
781 R Journal, 9(1), 421--436. URL https://journal.r-project.org/archive/2017/RJ-2017-
782 016/index.html.
783 Hamdan, K., Schmidt, M. G., 2012. The influence of bigleaf maple on chemical properties of
784 throughfall, stemflow, and forest floor in coniferous forest in the Pacific Northwest. Can. J.
785 For. Res., 42(5), 868-878.
786 Head, K.H., Epps, R.J., 2011. Manual of Soil Laboratory Testing: Permeability. Shear
787 Strenght and Compressibility Tests, vol. 2. CRC Press, Boca Raton.
788 Herwitz, S. R., 1986. Infiltration-excess caused by stemflow in cyclone prone tropical
789 rainforest. Earth Surface Processes and Landforms, 11, 401-412.
790 in Forested Ecosystems. In: *Forest Hydrology and Biogeochemistry: Synthesis of Past*
791 *Research and Future Directions, Ecol. Stud. Ser.* Vol. 216, edited by Levia, D. F., Carlyle-
792 Moses, D. E., Tanaka, T., pp. 483-498, Springer, Heidelberg.
793 Johnson, M. S., Jost, G., 2011. Ecohydrology and Biogeochemistry of the Rhizosphere
794 Johnson, M. S., Lehmann, J., Riha, S., Krusche, A. V., Richey, J. E., Ometto, J.P., Couto, E.
795 G., 2008. CO_2 efflux from Amazonian headwater streams represents a significant fate for
796 deep soil respiration. Geophysical Research Letters, 35, L17401.
797 Johnson, M. S., Lehmann, J., 2006. Double-funnelling of trees: Stemflow and root-induced
798 preferential flow. Ecoscience, 13(3), 324-333.
799 Kattge, J. et al., 2011. TRY – a global database of plant traits. Global Change Biology, 17,
800 2905-2935.
801 Kuhn, M. et al., 2018. caret: Classification and Regression Training. R package version
802 6.0.81. https://CRAN.R-project.org/package=caret
803 Kuzyakov, Y., Blagodatskaya, E., 2015. Microbial hotspots and hot moments in soil: Concept
804 & review. Soil Biology & Biochemistry, 83, 184-199.
805 Lemon, P., E., 1956. A Spherical Densiometer For Estimating Forest Overstory Density.
806 Forest Sci. 2, 314-320.
807 Levia, D. F., Frost, E.E., 2003. A review and evaluation of stemflow literature in the
808 hydrologic and biogeochemical cycles of forested and agricultural ecosystems. J. Hydrol.,
809 274(1-4), 1-29.

Levia, D. F., Germer, S., 2015. A review of stemflow generation dynamics and stemflow-environment interactions in forests and shrublands. Rev. Geophys., 53, 673-714.

Levia, D. F., Herwitz, S. R., 2000. Physical properties of stemflow water in relation to leachate dynamics: Implications for nutrient cycling. Can. J. For. Res., 30(4), 662-666.

Levia, D. F., Keim, R. F., Carlyle-Moses, D. E., Frost, E. E., 2011. Throughfall and stemflow in wooded ecosystems. In: *Forest Hydrology and Biogeochemistry: Synthesis of Past Research and Future Directions, Ecol. Stud. Ser.* Vol. 216, edited by Levia, D. F., Carlyle-Moses, D. E., Tanaka, T., pp. 425-443, Springer, Heidelberg.

Levia, D. F., van Stan, J. T., Inamdar, S. P., Jarvis, M. T., Mitchell, M. J., Mage, S. M., Scheick, C. E., McHale, P. J., 2012. Stemflow and dissolved organic carbon cycling: Temporal variability in concentration, flux, and UV-vis spectral metrics in a temperate broadleaved deciduous forest in the eastern United States. Can. J. For. Res., 42(1), 207-216.

Levia, D. F., Van Stan, J. T., Mage, S. M., Kelley-Hauske., 2010. Temporal variability of stemflow volume in a beech-yellow poplar forest in relation to tree species and size. J. Hydrol., 380(1-2), 112-120.

Levia. D. F., Michakzik, B., Bischoff, S., Richter, S., Legates, D. R., 2015. Differential stemflow yield from European beech saplings: The role of individual canopy structure metrics. Hydrol. Process., 29(1), 43-51.

Liang, W. L., Kosugi, K., and Mizuyama, T., 2009. A three-dimensional model of the effect of stemflow on soil water dynamics around a tree on a hillslope, J. Hydrol., 366(1-4), 62-75.

Liang, W. L., Kosugi, K., and Mizuyama, T., 2015. Soil water redistribution process around a tree on a hillslope: The effect of stemflow on the drying process, Ecohydrology, 8, 1381-1395.

Liang, W. L., Kosugi, K., Mizuyama, T., 2007. Heterogenous soil water dynamics around a tree growing on a steep hillslope. Vadose Zone J., 6(4), 879-889.

Liang, W., Kosugi, K., Mizuyama, T., 2011. Soil water dynamics around a tree on a hillslope with or without rainwater supplied by stemflow. Water Resour. Res. 47 (W02541).

Liu, J., Engel, B. A., Wang, Y., Wu, Y., Zhang, Z, Zhang, M., 2019. Runoff response to soil moisture and micro-topographic structure on the plot scale. Scientific Reports, 9(1), 2532.

Lloyd, J., Taylor, J. A., 1994. On the temperature dependence of soil respiration. Functional Ecology, 8, 315-323.

Lu, N., Godt, J., 2013. Hillslope Hydrology and Stability. Cambridge University Press, New York.

Lu, N., Likos, W.J., 2004. Unsaturated Soil Mechanics. John Wiley and Sons, Hoboken, US.

Martinez-Meza, E., Whitford, W. G., 1996. Stemflow, throughfall and channelization of stemflow by roots in three Chihuahuan desert shrubs. J. Arid Environ., 32(3), 271-287.

McClain, M. E. Boyer, E. W., Dent, C. L., Gergel, S. E., Grimm, N. B., Groffman, P. M., Hart, S. C., Harvey, J. W., Johnston, C. A., Mayorga, E., 2003. Biogeochemical hot spots and hot moments at the interface of terrestrial and aquatic ecosystems. Ecosystems, 6(4), 301-312.

Mein, R.G., Larson, C.L., 1973. Modeling infiltration during steady rain. Water Resour. Res. 9 (2), 384–394.

Meinzer, F. C., Lachenbruch, B., Dawson, T., E. (Eds.), 2011. *Size- and Age-Related Changes in Tree Structure and Function*. Tree Physiology, Vol. 4. Springer, Heidelberg.

Miyata, S. K., Kosugi, K., Gomi, T., Mizuyama, T., 2009. Effects of forest floor coverage on overland flow and soil erosion on hillslopes in Japanese cypress plantation forests. Water Resour. Res., 45, W06402.

Molina, A., del Campo, A. D., 2012. The effects of experimental thinning on throughfall and stemflow: a contribution towards hydrology-oriented silviculture in Aleppo pine plantations. For. Ecol. Manage., 269, 2016-213.

Nespoulus, J., Merino-Martin, L., Monier, Y., Bouchet, D., Ramel, M., Dombey, R., Viennois, G., Mao, Z., Zhang, J., Cao, K., Le Bissonnais, Y., Sidle, R., Stokes, A., 2019. Tropical forest structure and understorey determine subsurface flow through biopores formed by plant roots. Catena, In Press.

Norris, J.S. et al., 2008. Slope Stability and Erosion Control: Ecotechnological Solutions. Springer, Doerdrecht.

Novick, K. A. et al., 2016. The increasing importance of atmospheric demand for ecosystem water and carbon fluxes. Nature Climate Change, NCLIMATE3114

Partington, D., Brunner, P., Frei, S., Simmons, C. T., Werner, A. D., Therrien, R., Maier, H. R., Dandy, G. C., Fleckenstein, J. H., 2013. Interpreting streamflow generation mechanisms from integrated surface-subsurface flow models of a riparian wetland and catchment. Water Res. Research, 49, 5501-5519.

Pasta, S., de Rigo, D., Caudullo, G., 2016. Acer pseudoplatanus in Europe: distribution, habitat, usage and threats. In: San-Miguel- Ayanz, J., de Rigo, D., Caudullo, G., Houston Durrant, T., Mauri, A. (Eds.), *European Atlas of Forest Tree Species*. Publ. Off. EU, Luxembourg.

876 Preti, F., Dani, A., Laio, F., 2010. Root profile assessment by means of hydrological,
877 pedological and above-ground vegetation information for bio-engineering purposes. Ecol.
878 Eng. 36, 305–316.
879 R Core Team, 2018. R: A language and environment for statistical computing. R Foundation
880 for Statistical Computing, Vienna, Austria. URL https://www.R-project.org/.
881 Rosier, C. L., Levia, D. F., van Stan, J. T., Aufdenkampe, A., Kan, J., 2016. Seasonal
882 dynamics of the soil microbial community structure within the proximal area of tree boles:
883 Possible influence on stemflow. European Journal of Soil Biology, 73, 108-118.
884 Rossi, R. E., Mulla, D. J., Journel, A. G., Franz, E. H., 1992. Geostatistical Tools for
885 Modeling and Interpreting Ecological Spatial Dependence. Ecological Monographs, 62(2),
886 277-314.
887 Schindlbacher, A., Rodler, A., Kuffner, M., Kitzler, B., Sessitsch, A., & Zechmeister-
888 Boltenstern, S. (2011). Experimental warming effects on the microbial community of a
889 temperate mountain forest soil. Soil biology & biochemistry, 43(7), 1417–1425.
890 doi:10.1016/j.soilbio.2011.03.005
891 Schwärzel, K., Ebermann, S., Schalling, N., 2012. Evidence of double-funnelling effect of
892 beech by visualization of flow pathways using dye tracer. J. Hydrol. 470-471, 184-192.
893 Shumway, R. H., Stoffer, D. S., 2017. *Time Series Analysis and Its Applications: With R*
894 *Examples*. Springer Texts in Statistics. Springer, Heidelberg.
895 Spencer, S. A., van Meerveld, H. J., 2016. Double funnelling in a mature coastal British
896 Columbia forest: spatial patterns of stemflow after infiltration. Hydrol. Process., 30, 4185-
897 4201.
898 Tanaka, N., Levia, D., Igarashi, Y., Yoshifuji, N., Tanaka, K., Tantasirin, C., Nanko, K.,
899 Suzuki, M., Kumagai, T., 2017. What factors are most influential in governing stemflow
900 production from plantation-grown teak trees? J. Hydrol., 544, 10-20.
901 Tardio, G., Gonzalez-Ollauri, A., Mickovski, S.B., 2016. A non-invasive root distribution
902 analysis methodology from a slope stability approach. Ecol. Eng. 97, 46–57.
903 Therneau, T., Atkinson, B., 2018. rpart: Recursive Partitioning and Regression Trees. R
904 package version 4.1-13. https://CRAN.R-project.org/package=rpart
905 US.
906 van Stan, J. T., Levia, D. F., Inamdar, S. P., Lepori-Buib, M., Mitchelle, M. J., 2012. The
907 effects of phenoseason and storm characteristics on throughfall solute washoff and leaching
908 dynamics from a temperate deciduous forest canopy. Science of the Total Environment, 430,
909 48-58.

910 Vanapalli, S.K., Fredlund, D.G., Pufahl, D.E., Clifton, A.W., 1996. Model for the prediction
911 of shear strength with respect to soil suction. Can. Geotech. J. 33, 379–392.
912 voor de Poorte, P., 2018. Retrieved 01 04, 2019, from PEDROX, live weather from
913 Catterline: <http://www.pedrox.com>.
914 Wang, L., Manzoni, S., Ravi, S., Rivero-Iregui, D., Caylor, K., 2015. Dynamic interactions of
915 ecohydrological and biogeochemical processes in water-limited systems. Ecosphere, 6(8),
916 Article 133
917 Wang, W. et al., 2016. Evaluation of air–soil temperature relationships simulated by land
918 surface models during winter across the permafrost region. The Cryosphere, 10, 1721-1737.
919 Whitford, W. G., Anderson, J., Rice, P. M., 1997. Stemflow contribution to the 'fertile
920 island' effect in creosotebush, *Larrea tridentate*. Journal of Arid Environments, 35, 451-457.
921 Wolf, D., Carson, E.A., Brown, R.H., 1972. Leaf area index and specific leaf area
922 determinations. J. Agron. Educ. 1, 24–27.
923 Wright, I. J., Reich, P. B., Cornelissen, J. H. C., Falster, D. S.,, Groom, P. K., Hikosaka, K.,
924 Lee, W., Lusk, C. H., Niinemets, U., Oleksyn, J., Osada, N., Poorter., H., Warton, D. I.,
925 Westoby, M., 2005. Modulation of leaf economic traits and trait relationships by climate.
926 Global Ecol. Biogeogr., 14, 411–421.
927 Wua, L., McGechanb, M.B., McRobertsc, N., Baddeleya, J.A., Watsona, C.A., 2007.
928 SPACSYS: Integration of a 3D root architecture component to carbon, nitrogen and water
929 cycling—Model description. Ecological Modelling, 200, 343-359.
930 Yuan, C., Gao, G., Fu, B., 2017. Comparisons of stemflow and its bio-/abiotic influential
931 factors between to xerophytic shrub species. Hydrol. Earth Syst. Sci., 21, 1421-1438.
932 Zimmermann, A., Zimmermann, B., 2014. Requirements for throughfall monitoring: the roles
933 of temporal scale and canopy complexity. Agric. For. Meteorol. 189–190, 125–139.
934
935